agriculture

MDPI

Article

Trichoderma Biocontrol Performances against Baby-Lettuce Fusarium Wilt Surveyed by Hyperspectral Imaging-Based Machine Learning and Infrared Thermography

Gelsomina Manganiello [1], Nicola Nicastro [2], Luciano Ortenzi [3,4], Federico Pallottino [4], Corrado Costa [4] and Catello Pane [2,*]

[1] Department of Agricultural Sciences, University of Naples Federico II, 80055 Portici, Italy; gelsomina.manganiello@unina.it
[2] Consiglio per la Ricerca in Agricoltura e l'analisi Dell'economia Agraria (CREA), Centro di Ricerca Orticoltura e Florovivaismo, via Cavalleggeri 25, 84098 Pontecagnano Faiano, Italy; nicola.nicastro91@gmail.com
[3] Department of Agriculture and Forest Sciences (DAFNE), Tuscia University, Via S. Camillo De Lellis, s.n.c.—01100 Viterbo & Via Angelo Maria Ricci 35, 02100 Rieti, Italy; luciano.ortenzi@unitus.it
[4] Consiglio per la Ricerca in Agricoltura e l'analisi dell'economia Agraria (CREA), Centro di Ricerca Ingegneria e Trasformazioni Agroalimentari, via Della Pascolare 16, 00015 Monterotondo, Italy; federico.pallottino@crea.gov.it (F.P.); corrado.costa@crea.gov.it (C.C.)
* Correspondence: catello.pane@crea.gov.it

Abstract: *Fusarium oxysporum* f. sp. *lactucae* is one of the most aggressive baby-lettuce soilborne pathogens. The application of *Trichoderma* spp. as biocontrol agents can minimize fungicide treatments and their effective targeted use can be enhanced by support of digital technologies. In this work, two *Trichoderma harzianum* strains achieved 40–50% inhibition of pathogen radial growth in vitro. Their effectiveness in vivo was surveyed by assessing disease incidence and severity and acquiring hyperspectral and thermal features of the canopies being treated. Infected plants showed a reduced light absorption in the green and near-red regions over time, reflecting the disease progression. In contrast, *Trichoderma*-treated plant reflectance signatures, even in the presence of the pathogen, converged towards the healthy control values. Seventeen vegetation indices were selected to follow disease progression. The thermographic data were informative in the middle–late stages of disease (15 days post-infection) when symptoms were already visible. A machine-learning model based on hyperspectral data enabled the early detection of the wilting starting from 6 days post-infection, and three different spectral regions sensitive to baby-lettuce wilting (470–490 nm, 740–750 nm, and 920–940 nm) were identified. The obtained results pioneer an effective AI-based decision support system (DSS) for crop monitoring and biocontrol-based management.

Keywords: digital agriculture; DSS; *Fusarium oxysporum* f. sp. *lactucae*; machine learning; multilayer feed forward artificial neural networks; precision biological control; *Trichoderma harzianum*

Citation: Manganiello, G.; Nicastro, N.; Ortenzi, L.; Pallottino, F.; Costa, C.; Pane, C. *Trichoderma* Biocontrol Performances against Baby-Lettuce Fusarium Wilt Surveyed by Hyperspectral Imaging-Based Machine Learning and Infrared Thermography. *Agriculture* **2024**, *14*, 307. https://doi.org/10.3390/agriculture14020307

Academic Editor: Roy Kennedy

Received: 30 October 2023
Revised: 9 February 2024
Accepted: 12 February 2024
Published: 14 February 2024

1. Introduction

Baby lettuce (*Lactuca sativa* L. var *acephala*) is among the most popular leafy vegetable consumed worldwide as ready-to-eat salads since it is low in calories, fat, and sodium and a good source of fiber, iron, folate, and vitamin C [1]. It is characterized by a very short growing cycle under polytunnels or greenhouses in intensive cropping systems characterized by high sowing densities, intense mechanization, sprinkling fertigation, little or no rotation, and a higher accumulated risk of pathogen inoculum. *Fusarium oxysporum* f. sp. *lactucae* (*Fol*) is one of the most feared soilborne fungal pathogens of this crop that is linked to the soil sickness syndrome [2,3]. This ascomycete was first isolated in Japan and described as a causal agent of root rot in lettuce in 1967 [4]; in Italy, it has been reported

as a Fusarium wilt agent in baby lettuce since 2001 [5]. *Fol* severely damages baby lettuce plants, causing marked stunting of growth, chlorosis and/or necrosis of the leaves, unmarketability of the harvested product, and even premature senescence and death. In the root system, no external symptoms are usually visible, but internally, a reddish-brown discoloration can be observed due to the pathogen's endophytic colonization of the vessels and their subsequent occlusion [6]. An early detection of *Fol* is necessary for plant health monitoring to better manage infections in the different stages of plant development, minimizing the risk of disease spreading and avoiding yield losses.

Innovative management of Fusarium wilt in baby lettuces aims to minimize the reliance on synthetic fungicides and enhance the application of environmentally friendly and agroecological strategies to meet the latest regulatory and commercial guidelines [7]. Biological control is a bioinspired crop protection method based on the use of beneficial microorganisms that are able to contain plant diseases through antagonistic mechanisms. Several microbial-based formulations, which include the antagonistic fungi *Trichoderma* spp. as an active ingredient, are registered and marketed worldwide as bio-fungicides due to their ability to contain important soil and foliar pathogens, such as *Fusarium*, *Sclerotinia*, *Botrytis*, and *Pythium* species [8]. The biocontrol actions of this fungus rely on various antagonistic mechanisms, including competition for space and nutrients, mycoparasitism, and the production of antimicrobial compounds [9,10]. In addition, *Trichoderma* spp. can establish positive interactions with plant roots, favoring water and nutrient uptake, increasing plant metabolism, and inducing plant defense responses [11,12].

The targeted use of high-performing antagonists combined with the early detection of outbreaks is crucial to achieve the effective biocontrol of baby-lettuce Fusarium wilt. Optoelectronic sensors, including hyperspectral and thermal cameras, can enable large-scale, rapid, and non-destructive image-based disease monitoring through remote interpretation models of spatially distributed information, which can be integrated into disease management procedures and support decision-making processes [13]. Image-based optoelectronic sensors work by acquiring data that can be traced back to the reflected portion of the electromagnetic spectrum (hyperspectral) or to the returned energy (thermal) from the plant surface in a specific wavelength range, whose spatial distribution is returned as a 2D image [14]. Fluctuations in band-to-band information are affected by the plant response to external stimuli as well as in response to physical–chemical and physiological changes [15]. The data produced need to be deeply analyzed, simplified, and modelized to extract the most useful information for practical applications [16,17]. In this context, machine learning (ML) techniques represent a fundamental step forward in data analytics since they allow us to extract synthetic information and use it to model the observed complex phenomena [18] in an efficient and comprehensive way. Recently, high-resolution hyperspectral imaging data were used to identify high-performing synthetic vegetational indices and to develop ML models that can trace and predict the biocontrol efficacy of a large collection of *Trichoderma* spp. against the soil-borne diseases caused by *Sclerotinia sclerotiorum* and *Sclerotium rolfsii* on baby lettuce [19]. However, in comparison to artificial intelligence studies based on optoelectronic data for disease detection, there are very few studies aimed at evaluating and rating biological control effectiveness. The early detection of plant diseases using digital pipelines, such as hyperspectral and infrared thermal imaging, is a complex task that must accurately address the concepts of diagnosis (catching differential characteristics) and monitoring (dynamics of symptom development) even under conditions with multiple interactions to which plants are generally exposed, such as those involving biological control agents [20]. The availability of datasets as representative as possible of the diverse conditions under which a disease can develop may be the major existing constraint of the digital imaging approach for plant disease detection [21].

Our study was aimed at identifying, biologically characterizing, assessing the biocontrol effectiveness against *Fol* on baby lettuce of two new *Trichoderma* isolates. The performances of these beneficial fungi were evaluated by both visual monitoring of disease progression, assessing disease incidence and severity, and by hyperspectral imaging and

infrared thermography, every 72 h for 18 days following pathogen inoculation. In addition, the hyperspectral data were used to train a ML predictive model to discriminate between diseased and healthy plants, starting from the early stages of pathogenesis. The obtained model allowed the objective evaluation of the selected antagonists' effectiveness in controlling plant wilting, confirming the transformative role of ML in redefining plant disease detection and management strategies.

2. Materials and Methods

2.1. Fungal Strains

Two different *Trichoderma* strains were isolated from suppressive soil. The fungi were subjected to monosporic culturing by serial ten-fold dilutions on potato dextrose agar (PDA) enriched with 0.1% Igepal colony constrictor and stored in the fungal collection of the CREA Research Centre for Vegetable and Ornamental Crops (Pontecagnano Faiano, Italy). *Trichoderma* isolates were maintained in potato dextrose broth (PDB, Condalab, Madrid, Spain) on a rotary shaker at 150 rpm for 96 h at 25 °C. Then, fresh mycelia were vacuum filtered through No. 4 Whatman filter paper (Whatman Biosystems Ltd., Maidstone, UK), frozen in liquid nitrogen, and ground into a fine powder using sterilized mortars and pestles. The samples were stored at −80 °C until DNA extraction. Total genomic DNA was extracted from 100 mg of the processed sample using the PureLink Plant Total DNA Purification Kit (Invitrogen™, ThermoFisher Scientific, Waltham, MA, USA) according to the manufacturer's protocol. PCR amplification of internal transcribed spacers (ITSs) and translation elongation factor 1α (TEF1) was performed in a Biorad C1000 Thermal Cycler (Bio-Rad, Hercules, CA, USA) following a previously reported PCR procedure [13]. Amplicons were purified by a PureLink™ PCR Purification Kit (Invitrogen™, ThermoFisher Scientific, Waltham, MA, USA), quantified by a NanoDrop™ (NanoDrop Technologies Inc., Wilmington, DE, USA), and sent for Sanger sequencing.

The fungal pathogen used in this study was *Fusarium oxysporum* f. sp. *lactucae* strain 18.4.2, which is stored in the fungal collection of the CREA Research Centre for Vegetable and Ornamental Crops (Pontecagnano Faiano, Italy).

2.2. Dual Culture Assay

The biocontrol activity of the two *Trichoderma* isolates was investigated in vitro against *Fol* through the dual culture approach following the same procedure reported in [19]. The inoculum consisted of a 0.5 cm diameter mycelial plug excised from the edges of a 7-day-old actively growing fungal culture of both the pathogen and *Trichoderma* strains. The plugs were placed simultaneously on the opposite borders of a new PDA plate (9 cm diameter), about 0.25 mm from the edges. As negative control, plates containing the pathogen alone were used. The plates were inoculated in triplicate and incubated at 25 °C; the radial growth was monitored each 24 h for 6 days post-inoculation (dpi). The growth inhibition percentage was calculated as follows:

$$\text{Inhibition (\%)} = 100 - \frac{\text{Control} - \text{DC}}{\text{Control}}$$

where Control = *Fol* radial growth in negative control and DC = *Fol* radial growth in the dual culture.

2.3. In Vivo Biocontrol Assay

Fol was stored at −80 °C as a conidial suspension in 30% glycerol, revived on PDA amended with 40 ppm streptomycin, and incubated at 25 °C. For root-dip inoculation of lettuce seedlings, an aqueous conidial suspension of 10^6 conidia mL^{-1} was prepared from 10-day-old cultures on PDA. One-liter flasks containing 200 g of common millet seeds were saturated with a 0.1 × PDB (*w*/*w*) solution and autoclaved. To prepare the *Trichoderma* inoculum, flasks were inoculated with 30 plugs (5 mm diameter) obtained from one-week-old plates of each antagonistic strain on PDA, and incubated for 15 days at 25 °C. At the

end of the incubation, the inoculum was ground and added to double sterilized peat soil at a final concentration of 2% (*w*/*w*). In the uninfected control, non-inoculated common millet, prepared as described above, was added. The inoculated and non-inoculated peat was wetted with sterile distilled water (250 mL kg^{-1} of peat) and incubated for 1 week in autoclavable plastic bags.

Baby lettuce seeds of the cultivar Aurora (Maraldi Sementi, Italy), which is susceptible to the *Fol* strain, were sown in sterile vermiculite-filled 500 mL trays, germinated in the dark at 25 °C, and then maintained in a growth chamber at 25 °C with a 12 h photoperiod. The irrigation was manually performed daily, distributing 100 mL of distillated water per tray and a basal NPK fertilizer was applied twice a week. After 15 days, the plants were transplanted into 100 mL plastic pots (7 cm Ø) filled with peat and inoculated as described above. The seedlings were removed from the vermiculite, rinsed in sterile water, and inoculated by root dipping into either sterile water (for uninfected control) or a conidial suspension of *Fol* for 20 min and transferred into a fresh pot containing sterile peat inoculated with the *Trichoderma* strains. The seedlings were incubated at 26 °C in a greenhouse for the next 18 days. Each treatment [reference healthy control (H), infected control (*Fol*), *T. harzianum* T2 strain (T2), *T. harzianum* Ts strain (Ts), and respective combined applications (T2 + *Fol*) and (Ts + *Fol*)] was performed on 10 pots (replicates) with one seedling each. The monitoring of disease development was performed every 72 h for the next 18 days (6 time points). For each time point, each pot was assessed for hyperspectral and thermal images, disease incidence (DI%), and severity index (DSI). For the DI (%) and DSI (%) calculations, the plants were randomly separated into 2 sub-groups of 5 seedlings each and the incidence was calculated as the percentage of symptomatic plants over the total number of plant in the subgroup, while DSI was assessed using a 0–3 severity scale adapted from Larkin et al. [22]: 0 = no symptoms, 1 = mild stunting, 2 = severe stunting and some leaf yellowing and/or necrosis, and 3 = dead plants (Figure 1).

The disease indices were calculated as follows:

$$\text{Disease incidence (DI\%)} = 100 \times \frac{\text{symptomatic plants}}{\text{total number of plants}}$$

$$\text{Disease severity (DSI\%)} = 100 \times \frac{\sum(\text{class frequency} \times \text{class score})}{\text{total number of observation} \times \text{max class score}}$$

At the end of the experiment (18 dpi), the plants were collected, and different biometric parameters were measured: leaf area index (LAI) using a leaf area meter (LI-3100C Area Meter, LI-COR®, Inc., Lincoln, NE, USA) and root and stem fresh and dry weights. The experiment was performed twice.

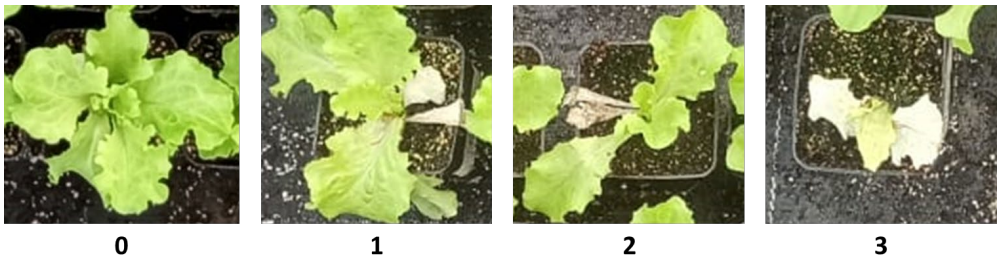

Figure 1. Representative photographs of the four baby-lettuce Fusarium wilt disease classes (0–3 severity scale).

2.4. Hyperspectral and Thermal Image Acquisitions

Hyperspectral images were acquired by a SPECIM IQ camera (Specim, Spectral Imaging Ltd., Oulu, Finland) in the 400–1000 nm range (204 wavelengths) with a 7 nm spectral resolution. The camera was equipped with a CMOS sensor with a spatial sampling size of 512 pixels and a 512 × 512-pixel image resolution (pixel size is 17.58 × 17.58 μm) and software for the automatic calculation of reflectance values. All the images were captured under daylight conditions in an irradiance range of 306–384 W m^{-2}. White reference,

dark frame, and raw data were acquired during all the measurements. Raw reflectance was calculated as reported by Pane et al. [13]. One image, each containing all the treatments (Control; *T. harzianum* Ts; *T. harzianum* T2; Ts + *Fol*; and T2 + *Fol*) for each replicate of the two repeated experiments (for a total of 20 samples per treatment) per time point, was acquired. The relative reflectance of the hyperspectral images was simultaneously computed by the camera software. Hyperspectral image elaborations were performed using R software version 4.1.2. Spectral graphics were generated by visualizing and extracting the hypercube dataset using the Raster R package [23]. The images were then classified following an unsupervised classification method by the Cluster R package, identifying 2 separate clusters, background, and plants. The background cluster was removed while a plant mask was applied for the extraction of 54 vegetational hyperspectral indices [24], averaging the pixel values for each replicate per treatment.

Thermal images were acquired, following the same experimental protocol conducted for hyperspectral acquisition, using a Flir T1030sc infrared camera (Flir System S.r.l.; Limbiate, Italy) with the following characteristics: IR sensor: 1024 × 768; detector type, Focal Plane Array uncooled microbolometer; field of view, 28° × 21°; image frequency, 120 Hz; spectral range, 7.5 to 14 μm; focus, automatic or manual; thermal sensitivity <20 mK at 30 °C; temperature range −40 +150 °C; thermal sensitivity (NETD) of < 20 mK. The squared shaped regions of interest (ROIs) were extracted from each plant image and the mean temperature ± standard deviation were calculated for each condition. The infrared camera acquired a thermal image along with an RGB spectrum. The two images did not perfectly overlap. A procedure based on an unsupervised k-means clustering algorithm was used to segmentate the RGB image to extract the plant areas. To make the RGB image overlap with the thermal image, a geometric morphometric procedure was applied. The images were superimposed using 4 type II landmarks that were easily identifiable in both the RGB and thermal images. Type II landmarks [25] are mathematical points whose claimed homology from case to case is supported only by geometric, not histological, evidence, for instance, the sharpest curvature of a leaf. The software TPSsuper allowed us to unwarp the thermal images to the RGB configuration (target shape).

Thus, the thermal images were aligned using the RGB landmark locations and were superimposed on the RGB image. The mask containing the part of the image with the plant, with the background subtracted using the k-means clustering algorithm on two clusters, was used to select the pixels for the plant in the thermal image.

2.5. Machine Learning Model

The statistical analysis approach chosen was based on ML applied to 240 samples, including 2 treatments (healthy control and *Fol*) for 6 time points (dpi) per 20 replicates (pots). Statistical modeling was applied to classify early *Fol*-infected samples from healthy controls starting from 3 dpi based on 204 hyperspectral reflectance values. Specifically, a multilayer feed forward artificial neural network (MLFN) was designed using a single hidden layer architecture with sigmoid activation functions and SoftMax output neurons. MLFN has been proven to be effective in interpreting hyperspectral vegetation signals [26]. The network was built with only a single layer with 15 neurons in the hidden layer [27] and was applied to the hyperspectral dataset with 204 features. The number of nodes was determined by convergence with respect to the accuracy of the training and test sets. The MLFN was trained using the gradient descent back propagation algorithm [28,29], implemented in the deep learning MATLAB (The MathWorks Inc. MA USA) toolbox. The dataset was partitioned using 80% of the samples (192) as the training set and the remaining 20% as the test set (48). This partitioning (equal for each group) was optimally chosen using the Euclidean distances calculated by the algorithm reported by Kennard and Stone [30] that selects parameters without a priori knowledge of a regression model. The cost function was minimized using the root mean squared (RMS) normalized error performance function with a 10^{-10} threshold on the gradient. Cross validation was also performed with 100 runs. To extract the most informative variables in distinguishing *Fol*-

infected from health samples, a study of the importance of hyperspectral features was also performed [31–33]. The model was developed by using the MATLAB 9.7 R2019b Deep Learning Toolbox. The model was then applied, as an external test, on the plant–*Trichoderma* and plant–*Trichoderma*–*Fol* combinations, with 20 samples per each treatment at different time points.

2.6. Statistical Analysis

Measurements of the pathogen growth inhibition in vitro, disease incidence, and disease severity were subjected to statistical analysis using GraphPad Prism Software. ANOVA was applied to evaluate the effects of the *Trichoderma* strains on the assessed parameters; the statistical analysis of variance was corrected for multiple comparisons by the Bonferroni hypothesis test, considering a p-value ≤ 0.05. Since an experiment effect was not observed, data from the repeated experiments were pooled and analyzed together.

Infrared thermographic data were analyzed by computing confidence intervals (p value ≤ 0.05), followed by a one-way analysis of variance (ANOVA), which was performed using the software package "Agricolae" in R version 4.1.2 [34]. Duncan's multiple-range test was used to analyze separated means with a cut-off for statistical significance at $p \leq 0.05$. A principal component analysis was carried out to select the most important vegetation indices according to the treatments and presence/absence of disease symptoms by using the "Factominer" package in the R software version 4.1.2 [35].

3. Results

3.1. Molecular Identification of Fungal Isolates

The *T. harzianum* and *F. oxysporum* f. sp. *lactucae* (*Fol*) isolates used in this study were identified by amplifying and sequencing molecular markers: internal transcribed spacer (ITS) and partial translated elongation factor 1α (TEF1) regions. Polymerase chain reactions produced amplicons of ~600 and 800 bp, respectively; they were sequenced by the Sanger method, and then separately compared against the non-redundant nucleotide database (nr/nt) in NCBI. The BLAST analyses revealed 99–100% nucleotide similarity to previously published *Trichoderma harzianum* strain sequences and 100% for the *F. oxysporum* f. sp. *lactucae* strain EFA 1186 (JQ219941.1). The sequences were deposited in GenBank under the following accession numbers: *Trichoderma harzianum* T2, OQ077191 (ITS) and OQ108506 (TEF1); *Trichoderma harzianum* Ts, OQ077192 (ITS) and OQ108507 (TEF1); *Fusarium oxysporum* f. sp. *lactucae* 18.4.2, OQ121825 (ITS) and OQ134872 (TEF1).

3.2. Trichoderma In Vitro Biocontrol Activity

The ability of *T. harzianum* strains to contain the development of *Fol* was assessed by an in vitro assay. The test was monitored every 24 h for 6 days, measuring the radial growth of the two microorganisms. As shown in Figure 2, *T. harzianum* Ts and T2 achieved a 40–50% inhibition of *Fol* radial growth starting from 48 h post-inoculation.

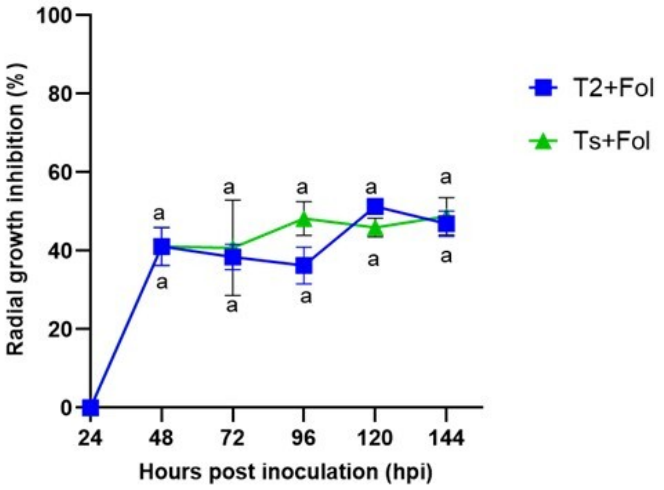

Figure 2. Radial growth inhibition (%) of *F. oxysporum f. sp. lactucae* challenged in vitro with *T. harzianum* Ts (green) and T2 (blue) strains, assessed daily for 144 h after plate inoculation. Different letters indicate significant differences between treatments ($p \leq 0.05$) according to ordinary two-way ANOVA followed by a Bonferroni's multiple comparison test.

No significant differences were observed among the different *Trichoderma* strains in inhibiting the phytopathogenic fungus over time. *Trichoderma* touched the pathogen within 5 days and mycelium overgrowth was observed after 7 days.

3.3. Trichoderma Biocontrol Activity In Vivo

The biological control ability of the two *T. harzianum* strains was further investigated by in vivo tests against *Fol* on green baby lettuce. Infected plants treated with the two beneficial fungi were checked every 72 h for 18 days, and the disease incidence and severity index percentages were assessed. The first symptoms were detected on 9 dpi as a slight leaf chlorosis. As time went on, the infected plants became stunted and progressively deteriorated, with leaf yellowing, necrosis, and severe growth and physiological alterations. The application of T2 significantly reduced the disease incidence starting from the appearance of symptoms (9 dpi) in comparison with the infected control (Figure 3A). In the last assessment, 70% of the T2-treated plants were symptomatic while for Ts-treated plants, the disease incidence was around 85%, which is comparable to the *Fol*-infected ones. Interestingly, both *T. harzianum* strains were able to slow the disease progression, with a 40% decrease in severity (Figure 3B). Overall, a significant *Trichoderma* treatment effect was found (p-value ≤ 0.0001). In general, the biotreated plants displayed lower levels of disease injuries or, in some cases, appeared asymptomatic (Figure 3A,B).

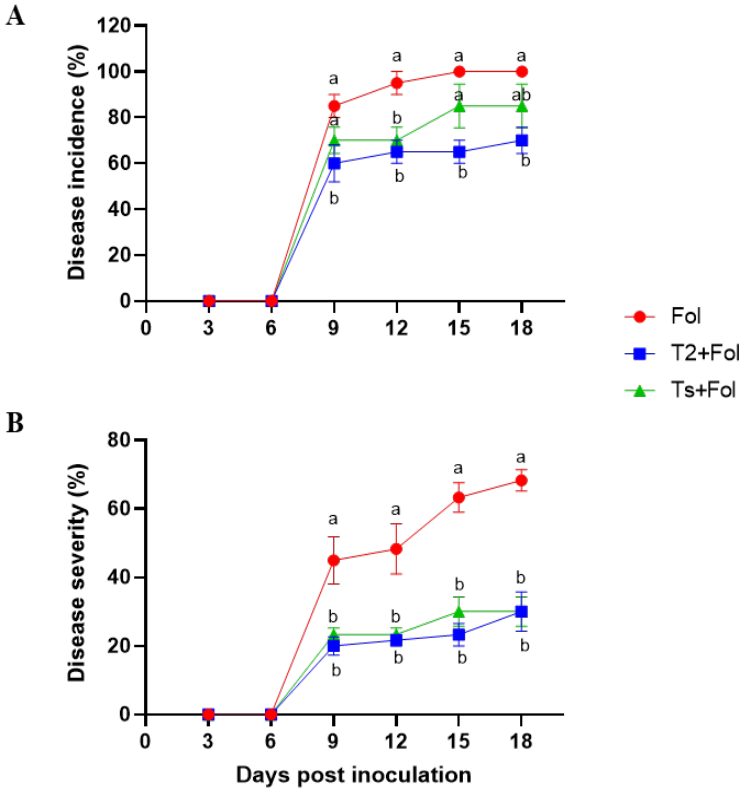

Figure 3. Effect of *T. harzianum* T2 (blue) and Ts (green) strains on incidence (**A**) and severity (**B**) of baby lettuce wilting caused by *F. oxysporum f. sp. lactucae* compared to the infected untreated control (red); monitored every three days for 18 days post-pathogen inoculation. Different letters indicate significant differences between treatments ($p \leq 0.05$) according to ordinary one-way ANOVA followed by a Bonferroni's multiple comparison test.

3.4. Effect of Trichoderma on the Growth of Infected and Healthy Plants

At the end of the experiment (18 dpi), the plants were collected and the leaf area index (LAI) and root and stem fresh and dry weights were assessed. The *Fol*-infected plants showed a 66% decrease in LAI compared to the untreated control, confirming that the pathogen strongly affected plant growth. On the other hand, the infected plants treated with *Trichoderma* had values comparable to that of healthy control (Figure 4A).

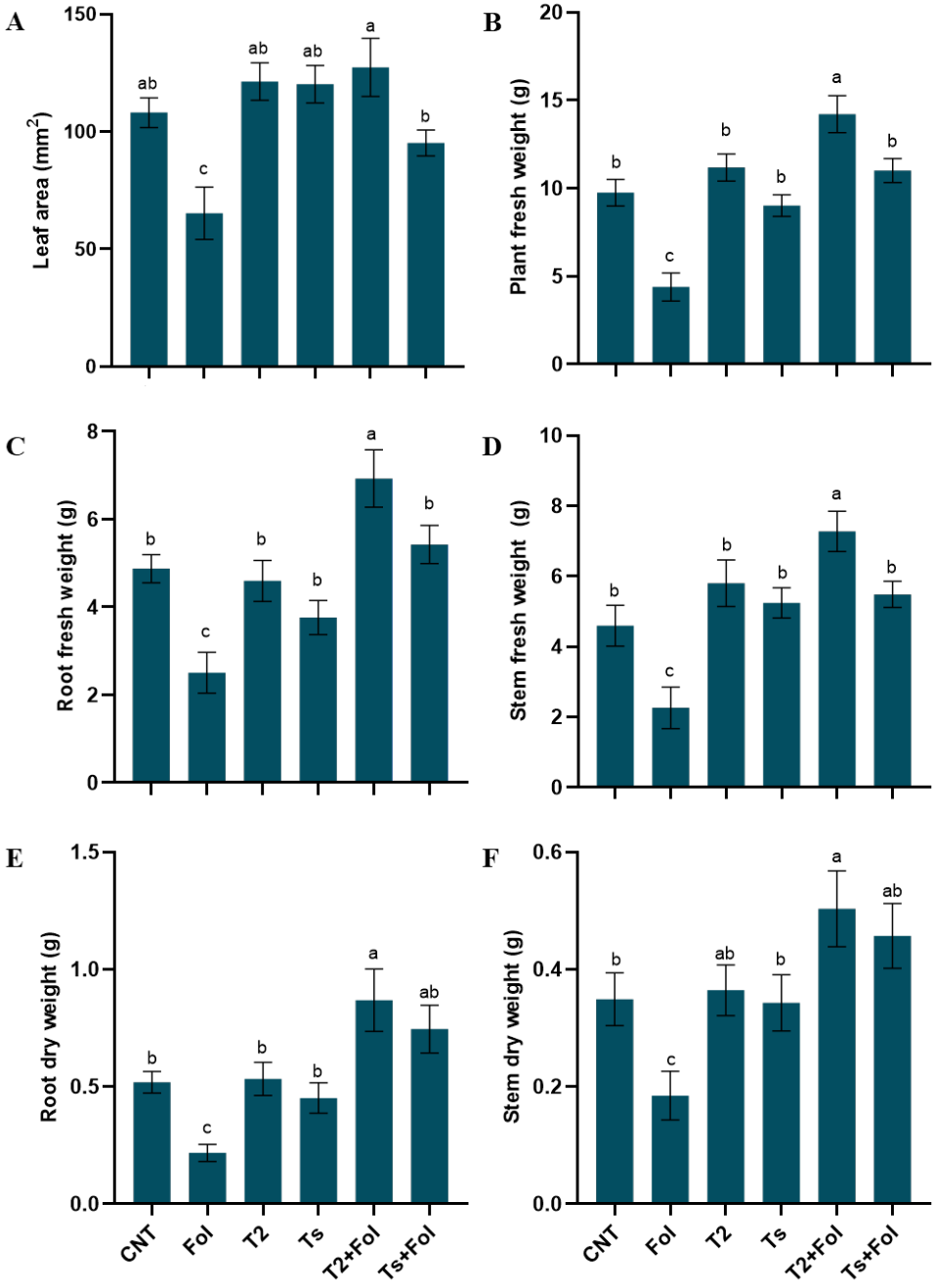

Figure 4. Biometric parameters, including leaf area (**A**), and plant fresh weight (**B**), root fresh and dry weights (**C**–**E**), and stem fresh and dry weights (**D**–**F**), assessed at the end of the in vivo experiment for untreated healthy (H) and infected (*Fol*) controls, plants treated with *T. harzianum* T2 and Ts strains, and their combinations with *Fol*. Different letters indicate significant differences between treatments ($p \leq 0.05$) according to ordinary one-way ANOVA followed by a Bonferroni's multiple comparison test.

Interestingly, no significant differences were observed when comparing infected and Ts-biotreated plants with uninfected biotreated plants (Ts + *Fol* vs. Ts) for all the analyzed biometric parameters. The application of T2 to infected plants resulted in a significant increase of all the assayed indicators (excluding leaf area) compared to biotreated and uninfected plants (T2 + *Fol* vs. T2). In terms of the whole plant fresh weight, T2 was the best performing treatment, with an increase of 35% and 70% compared to healthy and infected controls, respectively (Figure 4B). The fresh weight increase was associated with a more

than 100% increase both in the root and stem weights (T2 + *Fol* vs. *Fol*) (Figure 4C,D). Moreover, the fresh weight of plants treated with T2 and infected with *Fol* was significantly higher than those treated with T2. These differences were supported by the dry weight assessments, where significant differences were observed between infected and biotreated plants compared to both healthy and *Fol*-infected controls (Figure 4E,F). In this case, no significant differences were found between the T2 and Ts effects on *Fol*-infected plants.

3.5. Plant Reflectance and Thermographic Data

Infrared thermographic profiles were used for disease progression monitoring. The temperature variation (ΔT) was calculated by subtracting the values obtained from healthy control plants to those from bio-treated and infected plants. Early in the incubation period (3, 6, and 9 dpi), no significant differences were detected between bio-treated healthy plants and infected ones. At the following time point (12 dpi), a consistent ΔT increase was detected for T2-treated plants; at 15 dpi, the disease progression in *Fol*-infected plants produced a prominent ΔT increase, resulting in statistically significant differences compared to all the other treatments. In the last assessed time point (18 dpi), only T2-treated plants showed a ΔT that was considerably lower than the controls (Figure 5A,B). The reflectance profiles were calculated as the average of all pixel-wise spectral data from healthy, biotreated, infected, and infected/biotreated plants in the spectral range of 400–1000 nm, and are reported for each time point from 3 (no visible symptomatology) to 18 dpi (Figure 5C). Early in the incubation period (3 dpi), T2- and *Fol* + T2-treated plants showed reflectance values higher than healthy control and all the other treatments in the range between 500–600 nm (green region) and 750–1000 nm (NIR region). These differences appeared more consolidated in the following time points. At 9, 12, and 15 dpi, strong differences in reflectance values were recorded between T2, *Fol* + T2, *Fol*-infected, and uninfected plants. The spectral signatures of the diseased plants showed considerably lower reflectance levels in the NIR spectral region while T2- and *Fol* + T2-treated plants had reflectance values that were much higher than the uninfected control and all the other treatments in the green and NIR spectral regions. At 18 dpi, the spectral data of diseased plants and infected plants treated with Ts showed a pronounced decrease in the NIR region while the spectral signature of all the other treatment were flattened, similar to the uninfected control.

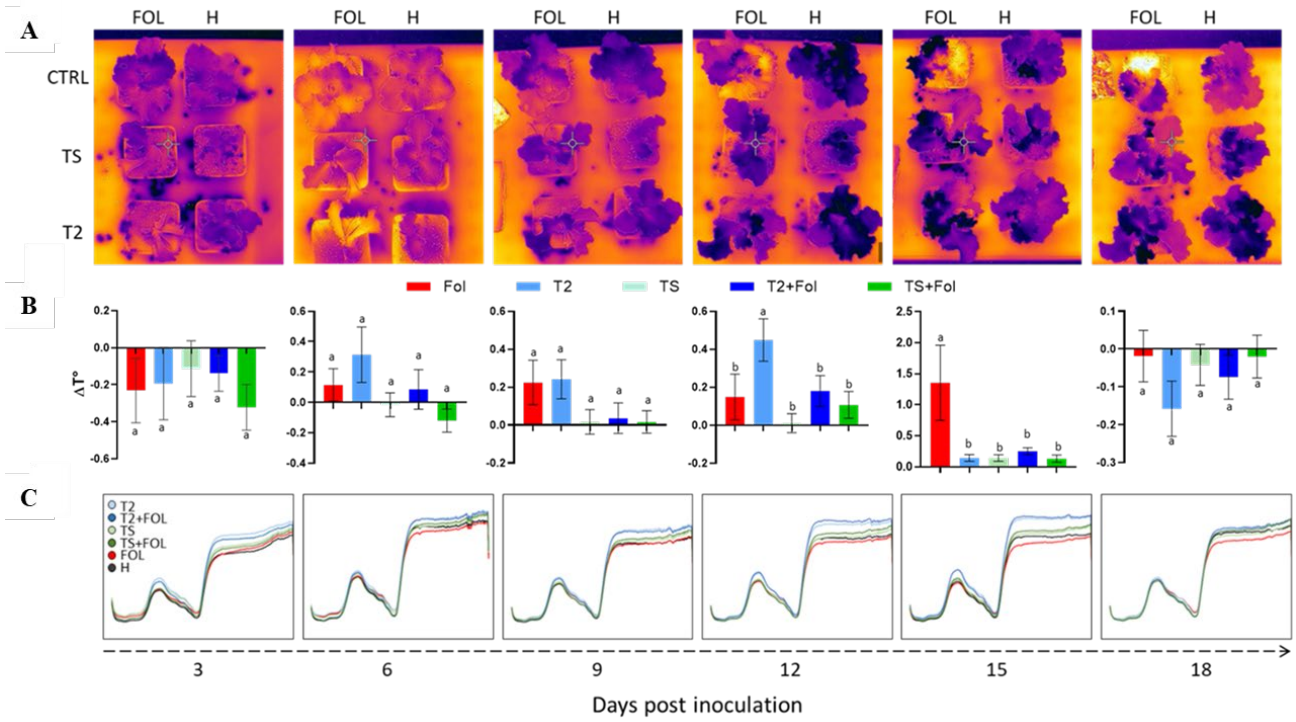

Figure 5. Thermal images (**A**) and trend over time of the thermographic parameter ΔT (**B**) during the in vivo experiment in untreated healthy (H) and infected (*Fol*) controls (CTRL), and treatments with *T. harzianum* T2 and Ts strains, and their combinations with *Fol*. Different letters indicate significant differences between treatments ($p \leq 0.05$) according to ordinary one-way ANOVA followed by a Bonferroni's multiple comparison test. Hyperspectral (400–1000 nm) reflectance signatures (**C**) acquired during the in vivo experiment for untreated healthy (H) and infected (*Fol*) controls, and treatments with *T. harzianum* T2 and Ts strains, and their combinations with *Fol* at each time point (3 to 18 dpi).

3.6. Hyperspectral VIs

The spectral signatures of the healthy, infected, and infected biotreated plants during the infection evolution were characterized using 54 hyperspectral VIs, known to be able to describe specific biochemical and/or physiological features of plants [36]. The selection of the most informative VIs was carried out by choosing them based on their correlation with principal component dimensions, in agreement with the observed disease severity index and ΔT°, as previously reported by Pane et al. [24].

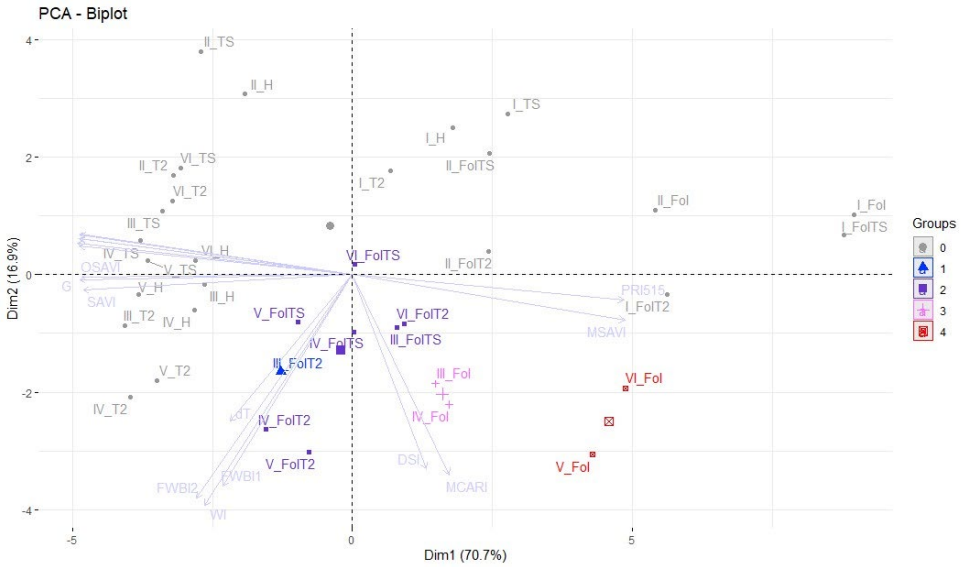

Figure 6. Principal component analysis biplot for visualizing distribution of healthy (H) and infected (Fol) controls, treatments with T. harzianum T2 and Ts strains, and their combinations with Fol at each assessment (3 to 18 dpi – I to VI), for the 16 selected vegetation indices (variables). X and Y axis show principal component 1 and principal component 2, explaining 70.7% and 16.9% of the total vari-ance, respectively. Color grouping was performed by considering the disease severity classes in the range 0 = healthy to 4 = highly infected.

As shown in Figure 6, the first two principal components (PCs) explained 87.6% of the total observed variance, 70.7% for PC1 and 16.9% for PC2, with eigenvalues higher than 1. PC1 was positively correlated with DVI (Difference Vegetation Index), SIPI (Structure Intensive Pigment Index 1), SRI (Simple Ratio Index), PSSRa (Pigment-Specific Simple Ratio a), G (Simple Ratio 550/670 Greenness Index), mSR705 (Modified Simple Ratio 705), OSAVI (Optimized Soil Adjusted Vegetation Index), RVSI (Red-Edge Stress Vegetation Index), SAVI (Soil-Adjusted Vegetation Index), NDVI (Normalized Difference Vegetation Index), and HVI (Hyperspectral Vegetation Index); it was negatively correlated with MSAVI (Modified Soil-Adjusted Vegetation Index) and PRI515 (Photochemical Reflectance Index) (corr. > 0.96). PC2 was positively correlated with MCARI (Modified Chlorophyll Absorption in Reflectance Index), WI (Water Index), FWBI1 (Floating-Position Water Band Index 1), and FWBI2 (Floating-Position Water Band Index 2) (corr. ≥ 0.7) and negatively correlated with WBI (Water band index) and the - vegetation indices for water stress. The symptomatic plants were separated along PC2, and the samples with the highest disease severity index (DSI 3 and 4) were organized in the negative side of PC1 and distributed along the positive flank of the second component.

3.7. Machine Learning Models

The results of the ML model for the early detection of *Fol*-infected samples (starting on 3 dpi) are shown in Table 1. The model reported a remarkably high accuracy in training (0% bad prediction) and in testing (6.3% bad prediction). Only three samples were misclassified: two *Fol*-treated samples at 6 dpi and one healthy one at 9 dpi. The standard deviation on the test accuracy obtained via cross validation was 0.06.

Table 1. Characteristics and principal results of the machine learning multi-layer feed forward artificial neural network (MLFN) model (training and internal tests) in predicting the classification of diseased vs. healthy samples from hyperspectral reflectance data at 6 days post inoculum (dpi).

Model Features	
Number of cases (training: 80%)	192
Number of hidden layers	1

Number of nodes	15
Number of epochs	30.000
% incorrect prediction (training: 80%)	0
Number of cases (internal test: 20%)	48
% incorrect prediction (internal test: 20%)	6.3%

Then, the trained model was applied as external test to the dataset including all plants under *Trichoderma*-based treatments both infected and not, for all the assessed time points (dpi). The classification results are reported in Table 2. Generally, the model highlighted higher number of plants classified as diseased in infected treatments than in non-infected ones. Interestingly, the model confirmed that *T. harzianum* T2 was the best performing strain, showing the lowest number of plants classified as diseased over time. Furthermore, in the first stages of pathogenesis (9 dpi, when mild symptoms were visible), samples classified as diseased resulted coherent with the disease incidence measured by visual assessment.

Table 2. Number of samples out of 20 for each *Trichoderma*-based treatment (T2, Ts, and combinations with *Fol*) that were classified as diseased by machine learning model at each time point (dpi).

Treatment	Number of Samples Classified as Diseased						
(dpi)	3	6	9	12	15	18
T2 + *Fol*	4	9	10	3	2	12
Ts + *Fol*	2	11	16	8	7	16
T2	2	1	0	0	0	0
Ts	1	4	4	1	0	2

The feature importance, plotted as a function of the wavelength, is shown in Figure 7. This values, extracted directly from the model trained parameters, returns the feature's largest contribution to the ML model and is higher the more sensitive a given wavelength is in determining whether the spectrum belongs to the *Fol* category or not. Considering a feature importance threshold of 0.7, three ranges of greater importance were found and are located at 470–490 nm, 740–750 nm, and 920–940 nm.

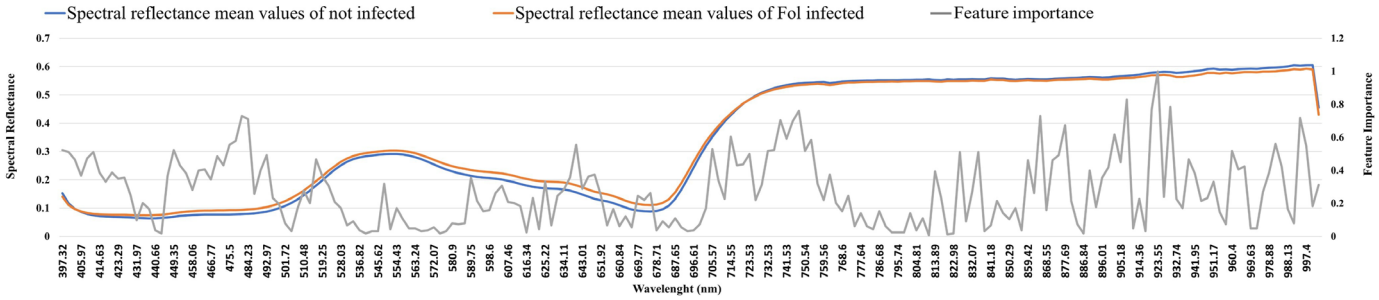

Figure 7. VIS–NIR spectral reflectance mean values of healthy (blue) and *Fol*-infected (orange) plant samples. Normalized feature importance values (grey) of the machine learning model are reported on the right axis.

4. Discussion

Biological control is an eco-friendly disease management alternative or it can supplement the use of conventional means based on synthetic pesticides [37]; however, it needs to be designed for each specific pathosystem. Baby lettuce tracheofusariosis is a very insidious fungal condition that is difficult to control, especially in the post-infection stages due to the endophytic progression of the pathogen. The hyperparasite *Trichoderma* can be explored as an effective containment strategy based on the wide range of antagonistic/fitness capabilities that these fungi could deploy, including rhizosphere competence, rapid site/niche colonization, multitrophic interactions, and activation of plant defenses [38–40].

The *T. harzianum* T2 and Ts strains significantly inhibited the in vitro mycelial radial growth of *F. oxysporum* f. sp. *lactucae*, and a consistent overgrowth was observed after 7 days of incubation in the dual culture assay. *Trichoderma* hyperparasitism is related to the production of lytic enzymes and/or other bioactive metabolites, the envelopment of host hyphae, and the development of appressorium-like structures propaedeutic to the penetration of the host cell wall [10,41–43]. The in vivo assay showed a significant ability of both antagonists to control baby lettuce wilt with an up to 40% reduction in disease severity compared to the unprotected control. *T. harzianum* T2 proved to be the best performing strain in reducing the stunted growth and yellowing symptoms which was supported by significant increases in biometric measurements, such as the leaf area and fresh and dry weights. However, both *Trichoderma* strains showed a specialized antagonistic attitude since in absence of the pathogen, they did not show any growth promotion effect compared to the uninfected control.

Optoelectronic sensing technologies, such as hyperspectral and thermal imaging, were successfully used in many studies aimed at plant phenotyping, contactless disease detection, and high-throughput monitoring, as they can capture (through canopy reflectance or thermography) plant physiological changes in response to external biotic or abiotic stimuli and/or stresses [24,44–46].

Here, the reflectance profiles of healthy and *Fol*-infected baby lettuces subjected to *Trichoderma* treatments, coupled to thermal signal acquired in passive mode, were used to follow the plants' responses during disease course.

During the infection, *Fol*-inoculated plants tended towards a slight reduction in light absorption in the green region and near the red-edge region, which are linked to changes in pigmentation and photosynthetic functions [47,48]. The consistently higher absorption in the NIR indicates the occurrence of anomalies in cell structure and water balance [47,48]. On the contrary, the reflectance signatures of *Trichoderma*-treated plants, even in the presence of the pathogen, tended to converge to signatures similar to the healthy controls over time. Generally, *F. oxysporum* only induces physiological changes and host-specific responses in the first stages of infection [49]; however, here, markedly visible symptoms occurred after approximately 9 dpi. Accordingly, noteworthy shifts in NIR reflectance were already detected at 6 dpi under T2 and *Fol* treatments, suggesting that infection by the pathogen and colonization by the *Trichoderma* strain are correlated with reflectance shifting in the NIR region during early stages of the interaction [50], probably due to the activation of plant–microorganism recognition mechanisms [51].

It was notable that the canopy reflectance of both healthy and infected plants treated with *T. harzianum* T2 suddenly increased in the green region and NIRin the early stages. Thermography also showed positive ΔT values for both *T. harzianum* T2-treated and *Fol*-infected plants, albeit in a more advanced symptomatic phase, at 12 and 15 dpi, respectively. As a matter of fact, Sun et al. [52] observed a similar delay in increasing leaf thermographic temperature changes 8 days after the start of an infection of *Cucumis sativus* with *F. oxysporum* f. sp. *cucumerinum,* when the leaves were lightly wilted. The authors discussed that the plant symptoms are related, in the early stages of pathogenesis, to chloroplast malformations and a loss of functionality, and later to the lack of water content in the leaves, which is detectable in IR (infra-red) images. The photosynthetic rate reduction observed in Fusarium-infected plants was attributed to stomatal closure and a reduction in both mesophyll conductance and Rubisco activity [53–55]. Recently, Navarro et al. [34] found substantial differences in the early spectra response of wild rocket affected by tracheofusariosis in comparison to other biotic and abiotic stressors, which was characterized by significant lowering of the chlorophyll a and b and carotenoid content. Pane et al. [25] interpreted, using hyperspectral data, the sequence of events occurring during wild rocket tracheofusariosis infection. At the start of pathogenesis, shifts in the absorption regions of chlorophyll (blue and red light) occur, while during the pathogen's endophytic colonization, wavelengths in the near-infrared range become sensitive to changes in biochemistry and cell structure and in water content. As *F. oxysporum* advances via the xylem, there is a

concurrent callose barrier formation (a plant reaction to the pathogen invasion), upward water flow is reduced, and tissues become dehydrated [56]. Only at 9 dpi, when wilting symptoms were already visible, *Fol*-infected plants showed a higher thermographic temperature than healthy plants but it was still lower than that of *T. harzianum* T2-treated ones; at 15 dpi, a significant increase in temperature was recorded for *Fol*-infected plants compared to all the other treatments. At the end of the experiment (18 dpi), all plants had a thermographic temperature comparable to the untreated control, except for *T. harzianum* T2-treated plants, which showed the lowest temperature.

T. harzianum T2 strongly affected the plant responses during the pathological assay. This effect should not be surprising since it is known that the direct interaction between pathogenic or beneficial microorganisms with plants can be similar and for example, may induce the production of several molecules able to prime defense mechanisms and trigger an innate immune response [57]. *Trichoderma*–plant interactions follow their own zigzag model [38,58]. In the early stages of contact, the plant activates several responses after *Trichoderma* recognition by pattern recognition receptors (PRRs) that are able to distinguish microbe-associated molecular patterns (MAMPs). In this phase, an oxidative burst, callose deposition, reactive oxygen species (ROS) signaling, and systemically transmitted stomatal closure are induced since the host is not able to distinguish *Trichoderma* as a friendly colonizer [59]. All these mechanisms could explain the spectral shifts and ΔT° increase observed in *T. harzianum* T2-biotreated plants, suggesting an effect on priming activation.

A pattern of baby lettuce–*Fusarium*–*Trichoderma* interactions also emerged from the PCA plot of spectral features of plants under the different treatments over time. It was largely due to disease severity (70.7% of variability) that proved to be associated with hyperspectral VIs that are closely linked to plant vitality and chlorophyll alterations, such as PRI515, MCARI, and SAVI. On the other hand, the residual variability (16.9%) can be explained by VIs closely linked to water status, such as FWBI1, FWBI2, WBI, and WI. Interestingly, *T. harzianum* T2-treated plants tended to have a higher correlation at each time point. ML performed by submitting the hyperspectral data cube to a multilayer feed forward artificial neural network managed to detect diseased plants at an early stage, achieving a 93.7% success rate through a two-class model. According to the literature, the most useful spectral regions for a simple healthy/diseased plant discrimination are those linked to the chlorophyll content (460–500 nm), leaf cell integrity (730–760 nm), and biochemistry (900–940 nm) [24]. The simple model applied to the dataset from the *Trichoderma*-based treatments for *T. harzianum* Ts had a higher number of samples classified as positive than for the strain T2, confirming the best biocontrol performance for this antagonist.

5. Conclusions

In this study, two new strains of *T. harzianum* were identified and biologically characterized in relation to their ability to control *Fol* pathogenesis on baby lettuce. Both strains were effective in containing Fusarium wilt on the crop, with a 40–50% reductio in disease severity in comparison to the infected controls, at a laboratory scale. Changes in the leaf optical properties of biotreated baby lettuces in response to the pathogen and/or beneficial fungi revealed the high discriminatory potential for several VIs to distinguish between infected and non-infected plants and the poor timeliness of passive thermal imaging. Healthy conditions were linked to VIs related to chlorophyll pigments, vegetation, and plant vitality (DVI, SIPI, SRI, PSSRa, G, mSR705, OSAVI, RVSI, SAVI, NDVI, HVI, MSAVI, PRI515). On the other hand, diseased plants were clustered by VIs associated with water stress (WI, FWBI1, FWBI2). The spectral changes observed in plant–*Fol* and plant–*Trichoderma* interactions may be associated with physiological and biochemical leaf changes triggered by microbe recognition processes. The ML algorithm trained with the hyperspectral data enabled the early detection of Fusarium wilt on baby lettuce and allowed us to identify three different spectral regions that are sensitive to the disease progression (460–500, 730–760, and 900–940 nm). A few selected wavelengths/indices, based on these results,

could be implemented using simple and cheap sensors for in situ monitoring through spectral image acquisition of Fusarium wilted areas in intensive baby lettuce cultivation.

Author Contributions: Conceptualization, C.P. and C.C.; methodology, G.M. and C.P.; software, validation, and formal analysis, G.M., N.N., L.O., F.P., and C.C.; investigation, C.P. and G.M.; writing—original draft preparation, G.M., L.O., C.C., and C.P.; writing—review and editing, G.M., N.N., F.P., L.O., C.C., and C.P.; supervision, project administration, and funding acquisition, C.P. All authors have read and agreed to the published version of the manuscript.

Funding: This study was funded by the Italian Ministry for Agriculture, Food Sovereignty and Forestry (MASAF), through the sub-project 'Tecnologie digitali integrate per il rafforzamento sostenibile di produzioni e trasformazioni agroalimentari (AgroFiliere)' (AgriDigit programme) (DM 36503.7305.2018 of 20 December 2018).

Institutional Review Board Statement: Not applicable.

Data Availability Statement: The datasets used and/or analyzed during the current study are available from the corresponding authors on reasonable request.

Acknowledgments: Luciano Ortenzi, who developed and implemented the algorithms and performed the computations, acknowledges the framework of the Ministry of University and Research (MUR) initiative Departments of Excellence (Law 232/2016) DAFNE Project 2023-27 Digital, Intelligent, Green and Sustainable (acronym: D.I.Ver.So). Gelsomina Manganiello also acknowledges funding from PON R&I 2014-2020 (FSE REACT-EU) DM 1062 AZIONE IV.6 (CUP: E65F21003080003).

Conflicts of Interest: The authors declare no conflicts of interest.

References

1. Kim, M.J.; Moon, Y.; Tou, J.C.; Mou, B.; Waterland, N.L. Nutritional value, bioactive compounds and health benefits of lettuce (*Lactuca sativa* L.). *J. Food Compos. Anal.* **2016**, *49*, 19–34. https://doi.org/10.1016/j.jfca.2016.03.004.
2. Scott, J.C.; Gordon, T.R.; Shaw, D.V.; Koike, S.T. Effect of temperature on severity of Fusarium wilt of lettuce caused by *Fusarium oxysporum* f. sp. *lactucae*. *Plant Dis.* **2010**, *94*, 13–17. https://doi.org/10.1094/PDIS-94-1-0013.
3. Randall, T.E.; Fernandez-Bayo, J.D.; Harrold, D.R.; Achmon, Y.; Hestmark, K.V.; Gordon, T.R.; Stapleton, J.J.; Simmons, C.W.; Vander Gheynst, J.S. Changes of *Fusarium oxysporum* f.sp. *lactucae* levels and soil microbial community during soil biosolarization using chitin as soil amendment. *PLoS ONE* **2020**, *15*, e0232662. https://doi.org/10.1371/journal.pone.0232662.
4. Matuo, T.; Motohashi, S. On *Fusarium oxysporum* f. sp. *lactucae* N.F. causing root rot of lettuce. *T. Mycol. Soc. Jpn.* **1968**, *8*, 13–15.
5. Garibaldi, A.; Gilardi, G.; Gullino, M.L. First report of *Fusarium oxysporum* on lettuce in Europe. *Plant Dis*. **2002**, *86*, 1052–1052. https://doi.org/10.1094/PDIS.2002.86.9.1052B.
6. Gordon, T.R.; Koike, S.T. Management of Fusarium wilt of lettuce. *Crop. Prot.* **2015**, *73*, 45–49. https://doi.org/10.1016/j.cropro.2015.01.011.
7. United Nations. Department of Economic and Social Affairs. 2015. Available online: https://sdgs.un.org/2030agenda (accessed on 1 July 2023)
8. Guzmán-Guzmán, P.; Kumar, A.; de los Santos-Villalobos, S.; Parra-Cota, F.I.; Orozco-Mosqueda, M.d.C.; Fadiji, A.E.; Hyder, S.; Babalola, O.O.; Santoyo, G. Trichoderma Species: Our Best Fungal Allies in the Biocontrol of Plant Diseases—A Review. *Plants*. 2023, 12, 432. https://doi.org/10.3390/plants12030432.
9. Elad, Y. Biological control of foliar pathogens by means of *Trichoderma harzianum* and potential modes of action. *Crop. Prot*. **2000**, *19*, 709–714. https://doi.org/10.1016/S0261-2194(00)00094-6.
10. Howell, C.R. Mechanisms employed by *Trichoderma* species in the biological control of plant diseases: The history and evolution of current concepts. *Plant Dis.* **2003**, *87*, 4–10. https://doi.org/10.1094/PDIS.2003.87.1.4.
11. Harman, G.E.; Howell, C.R.; Viterbo, A.; Chet, I.; Lorito, M. *Trichoderma* species–Opportunistic, avirulent plant symbionts. *Nat. Rev. Microbiol*. **2004**, *2*, 43–56. https://doi.org/10.1038/nrmicro797.
12. Asad, S.A., 2022. Mechanisms of action and biocontrol potential of Trichoderma against fungal plant diseases - A review. *Ecological Complexity* 49, 100978. https://doi.org/10.1016/j.ecocom.2021.100978
13. Pane, C.; Manganiello, G.; Nicastro, N.; Cardi, T.; Carotenuto, F. Powdery mildew caused by *Erysiphe cruciferarum* on wild rocket (*Diplotaxis tenuifolia*): Hyperspectral imaging and machine learning modeling for non-destructive disease detection. *Agriculture* **2021**, *11*, 337. https://doi.org/10.3390/agriculture11040337.
14. Meola, C.; Carlomagno, G.M. Recent advances in the use of infrared thermography. *Meas. Sci. Technol*. **2004**, *15*, R27. https://doi.org/10.1088/0957-0233/15/9/R01.
15. Sarić, R.; Nguyen, V.D.; Burge, T.; Berkowitz, O.; Trtílek, M.; Whelan, J.; Lewsey, M.G.; Čustović, E. Applications of hyperspectral imaging in plant phenotyping. *Trends Plant Sci*. **2022**, *27*, 301–315. https://doi.org/10.1016/J.TPLANTS.2021.12.003.

16. Huang, Y.; Chen, Z.-X.; Yu, T.; Huang, X.-Z.; Gu, X.-F. Agricultural remote sensing big data: Management and applications. *J. Integr. Agric.* **2018**, *17*, 1915–1931. https://doi.org/10.1016/S2095-3119(17)61859-8.
17. Ma, Y.; Wu, H.; Wang, L.; Huang, B.; Ranjan, R.; Zomaya, A.; Jie, W. Remote sensing big data computing: Challenges and opportunities. *Future Gener. Comput. Syst.* **2015**, *51*, 47–60. https://doi.org/10.1016/J.FUTURE.2014.10.029.
18. Paoletti, M.E.; Haut, J.M.; Plaza, J.; Plaza, A. Deep learning classifiers for hyperspectral imaging: A review. *ISPRS J. Photogramm. Remote Sens.* **2019**, *158*, 279–317. https://doi.org/10.1016/j.isprsjprs.2019.09.006.
19. Pane, C.; Manganiello, G.; Nicastro, N.; Ortenzi, L.; Pallottino, F.; Cardi, T.; Costa, C. Machine learning applied to canopy hyperspectral image data to support biological control of soil-borne fungal diseases in baby leaf vegetables. *Biol. Control* **2021**, *164*, 104784.
20. Rieker, M.E.G.; Lutz, M.A.; El-Hasan, A.; Thomas, S.; Voegele, R.T. Hyperspectral Imaging and Selected Biological Control Agents for the Management of Fusarium Head Blight in Spring Wheat. *Plants* **2023**, *12*, 3534. https://doi.org/10.3390/plants12203534.
21. Ahmad, A.; Saraswat, D.; El Gamal, A. A survey on using deep learning techniques for plant disease diagnosis and recommendations for development of appropriate tools. *Smart Agric. Technol.* **2023**, *3*, 100083. https://doi.org/10.1016/j.atech.2022.100083.
22. Larkin, R.P.; Honeycutt, C.W. Effects of different 3-year cropping systems on soil microbial communities and Rhizoctonia diseases of potato. *Phytopathology* **2006**, *96*, 68–79. https://doi.org/10.1094/PHYTO-96-0068.
23. Hijmans, R.J.; Van Etten, J.; Cheng, J.; Mattiuzzi, M.; Sumner, M.; Greenberg, J.A.; Hiemstra, P.; Hingee, K.; Karney, C.; Mattiuzzi, M.; et al. Package "raster". *R Package* **2015**, *734*, 473.
24. Pane, C.; Manganiello, G.; Nicastro, N.; Carotenuto, F. Early detection of wild rocket tracheofusariosis using hyperspectral image-based machine learning. *Remote Sens.* **2022**, *14*, 84. https://doi.org/10.3390/rs14010084.
25. Slice, D.E. Introduction to landmark methods. In *Advances in Morphometrics*; Springer: Boston, MA, USA, 1996; pp. 113–115.
26. Moscovini, L.; Ortenzi, L.; Pallottino, F.; Figorilli, S.; Violino, S.; Pane, C.; Capparella, V.; Vasta, S.; Costa, C. An open-source machine-learning application for predicting pixel-to-pixel NDVI regression from RGB calibrated images. *Comput. Electron. Agric.* **2024**, *216*, 108536. https://doi.org/10.1016/j.compag.2023.108536.
27. Violino, S.; Benincasa, C.; Taiti, C.; Ortenzi, L.; Pallottino, F.; Marone, E.; Mancuso, S.; Costa, C. AI-based hyperspectral and VOCs assessment approach to identify adulterated extra virgin olive oil. *Eur. Food Res. Technol.* **2021**, *247*, 1013–1022. https://doi.org/10.1007/s00217-021-03683-4.
28. Dan Foresee, F.; Hagan, M.T. Gauss-newton approximation to bayesian learning. In Proceedings of the International Conference on Neural Networks (ICNN'97), IEEE, Houston, TX, USA, 12 June 1997; pp. 1930–1935.
29. MacKay, D.J.C. The evidence framework applied to classification networks. *Neural Comput.* **1992**, *4*, 720–736. https://doi.org/10.1162/neco.1992.4.5.720.
30. Kennard, R.W.; Stone, L.A. Computer aided design of experiments. *Technometrics* **1969**, *11*, 137–148. https://doi.org/10.1080/00401706.1969.10490666.
31. Antonucci, F.; Costa, C. Precision aquaculture: A short review on engineering innovations. *Aquac. Int.* **2020**, *28*, 41–57. https://doi.org/10.1007/s10499-019-00443-w.
32. Antonucci, F.; Manganiello, R.; Costa, C.; Irione, V.; Ortenzi, L.; Palombi, M.A. A quantitative multivariate methodology for unsupervised class identification in pistachio (*Pistacia vera* L.) plant leaves size. *Span. J. Agric. Res.* **2021**, *18*, e0208. https://doi.org/10.5424/sjar/2020184-16904.
33. Navarro, A.; Nicastro, N.; Costa, C.; Pentangelo, A.; Cardarelli, M.; Ortenzi, L.; Pallottino, F.; Cardi, T.; Pane, C. Sorting biotic and abiotic stresses on wild rocket by leaf-image hyperspectral data mining with an artificial intelligence model. *Plant Methods* **2022**, *18*, 45. https://doi.org/10.1186/s13007-022-00880-4.
34. de Mendiburu, F. Agricolae: Statistical Procedures for Agricultural Research. R Package Version 1.3-5. 2021. Available online: https://CRAN.R-project.org/package=agricolae (accessed on 3 January 2022).
35. Husson, F.; Josse, J.; Le, S.; Maintainer, J.M. *Package "Factominer" Title Multivariate Exploratory Data Analysis and Data Mining*; R Foundation for Statistical Computing: Vienna, Austria, 2020.
36. Xue, J.; Su, B. Significant remote sensing vegetation indices: A review of developments and applications. *J. Sens.* **2017**, *2017*, 1353691. https://doi.org/10.1155/2017/1353691.
37. Brotman, Y.; Kapuganti, J.G.; Viterbo, A. Trichoderma. *Curr. Biol.* **2010**, *20*, R390–R391.
38. Lorito, M.; Woo, S.L.; Harman, G.E.; Monte, E. Translational research on *Trichoderma*: From 'omics to the field. *Annu. Rev. Phytopathol.* **2010**, *48*, 395–417. https://doi.org/10.1146/annurev-phyto-073009-114314.
39. Vinale, F.; Flematti, G.; Sivasithamparam, K.; Lorito, M.; Marra, R.; Skelton, B.W.; Ghisalberti, E.L. Harzianic acid, an antifungal and plant growth promoting metabolite from *Trichoderma harzianum*. *J. Nat. Prod.* **2009**, *72*, 2032–2035. https://doi.org/10.1021/np900548p.
40. Nawrocka, lJ., Małolepsza, U., 2013. Diversity in plant systemic resistance induced by *Trichoderma*. *Biological Control* 67, 149-156. https://doi.org/10.1016/j.biocontrol.2013.07.005.
41. Lu, Z.; Tombolini, R.; Woo, S.; Zeilinger, S.; Lorito, M.; Jansson, J.K. In vivo study of *Trichoderma*-pathogen-plant interactions, using constitutive and inducible green fluorescent protein reporter systems. *Appl. Environ. Microbiol.* **2004**, *70*, 3073–3081. https://doi.org/10.1128/AEM.70.5.3073-3081.2004.
42. Harman, G.E. Overview of mechanisms and uses of *Trichoderma* spp. *Phytopathology* **2006**, *96*, 190–194. https://doi.org/10.1094/PHYTO-96-0190.

43. Sachdev, S.; Singh, R.P. *Trichoderma*: A multifaceted fungus for sustainable agriculture. In *Ecological and Practical Applications for Sustainable Agriculture*; Bauddh, K., Kumar, S., Singh, R., Korstad, J., Eds.; Springer: Singapore, 2020. https://doi.org/10.1007/978-981-15-3372-3_13.
44. Leucker, M.; Mahlein, A.-K.; Steiner, U.; Oerke, E.-C. Improvement of lesion phenotyping in *Cercospora beticola*–Sugar beet interaction by hyperspectral imaging. *Phytopathology* **2016**, *106*, 177–184. https://doi.org/10.1094/PHYTO-04-15-0100-R.
45. Zhang, J.; Cheng, T.; Shi, L.; Wang, W.; Niu, Z.; Guo, W.; Ma, X. Combining spectral and texture features of UAV hyperspectral images for leaf nitrogen content monitoring in winter wheat. *Int. J. Remote Sens.* **2022**, *43*, 2335–2356. https://doi.org/10.1080/01431161.2021.2019847.
46. Aviara, N.A.; Liberty, J.T.; Olatunbosun, O.S.; Shoyombo, H.A.; Oyeniyi, S.K. Potential application of hyperspectral imaging in food grain quality inspection, evaluation and control during bulk storage. *J. Agric. Food Res*. **2022**, *8*, 100288. https://doi.org/10.1016/j.jafr.2022.100288.
47. Haboudane, D. Hyperspectral vegetation indices and novel algorithms for predicting green LAI of crop canopies: Modeling and validation in the context of precision agriculture. *Remote Sens. Environ*. **2004**, *90*, 337–352. https://doi.org/10.1016/j.rse.2003.12.013.
48. Vescovo, L.; Wohlfahrt, G.; Balzarolo, M.; Pilloni, S.; Sottocornola, M.; Rodeghiero, M.; Gianelle, D. New spectral vegetation indices based on the near-infrared shoulder wavelengths for remote detection of grassland phytomass. *Int. J. Remote Sens.* **2012**, *33*, 2178–2195. https://doi.org/10.1080/01431161.2011.607195.
49. Bauriegel, E.; Herppich, W. Hyperspectral and chlorophyll fluorescence imaging for early detection of plant diseases, with special reference to *Fusarium* spec. infections on wheat. *Agriculture* **2014**, *4*, 32–57. https://doi.org/10.3390/agriculture4010032.
50. Marín-Ortiz, J.C.; Gutierrez-Toro, N.; Botero-Fernández, V.; Hoyos-Carvajal, L.M. Linking physiological parameters with visible/near-infrared leaf reflectance in the incubation period of vascular wilt disease. *Saudi, J. Biol. Sci*. **2020**, *27*, 88–99. https://doi.org/10.1016/j.sjbs.2019.05.007.
51. Woo, S.L.; Hermosa, R.; Lorito, M.; Monte, E. *Trichoderma*: A multipurpose, plant-beneficial microorganism for eco-sustainable agriculture. *Nat. Rev. Microbiol*. **2022**, *21*, 312–326. https://doi.org/10.1038/s41579-022-00819-5.
52. Sun, Y.; Wang, M.; Li, Y.; Gu, Z.; Ling, N.; Shen, Q.; Guo, S. Wilted cucumber plants infected by *Fusarium oxysporum* f. sp. *cucumerinum* do not suffer from water shortage. *Ann. Bot*. **2017**, *120*, 427–436. https://doi.org/10.1093/aob/mcx065.
53. Lorenzini, G.; Guidi, L.; Nali, C.; Ciompi, S.; Soldatini, G.F. Photosynthetic response of tomato plants to vascular wilt diseases. *Plant Sci.* **1997**, *124*, 143–152. https://doi.org/10.1016/S0168-9452(97)04600-1.
54. Saeed, I.A.M.; MacGuidwin, A.E.; Rouse, D.I.; Sharkey, T.D. Limitation to photosynthesis in *Pratylenchus penetrans*–and *Verticillium dahliae* -infected potato. *Crop. Sci*. **1999**, *39*, 1340–1346. https://doi.org/10.2135/cropsci1999.3951340x.
55. Costa Pinto, L.S.R.; Azevedo, J.L.; Pereira, J.O.; Carneiro Vieira, M.L.; Labate, C.A. Symptomless infection of banana and maize by endophytic fungi impairs photosynthetic efficiency. *New Phytol*. **2000**, *147*, 609–615. https://doi.org/10.1046/j.1469-8137.2000.00722.x.
56. Pshibytko, N.L.; Zenevich, L.A.; Kabashnikova, L.F. Changes in the photosynthetic apparatus during Fusarium wilt of tomato. *Russ. J. Plant Physiol*. **2006**, *53*, 25–31. https://doi.org/10.1134/S1021443706010031.
57. Gupta, R.; Bar, M. Plant immunity, priming, and systemic resistance as mechanisms for *Trichoderma spp.* Biocontrol. In *Trichoderma: Host Pathogen Interactions and Applications–Rhizosphere Biology*; Sharma, A.K., Sharma, P., Eds.; Springer: Singapore, 2020; pp. 81–110.
58. Jones, J.D.G.; Dangl, J.L. The plant immune system. *Nature* **2006**, *444*, 323–329. https://doi.org/10.1038/nature05286.
59. Morán-Diez, M.E.; de Alba, Á.E.M.; Rubio, M.B.; Hermosa, R.; Monte, E. *Trichoderma* and the plant heritable priming responses. *J. Fungi* **2021**, *7*, 318. https://doi.org/10.3390/jof7040318.